HHS Public Access

Author manuscript

Clin Cancer Res. Author manuscript; available in PMC 2019 October 15.

Published in final edited form as:

Clin Cancer Res. 2018 October 15; 24(20): 5058–5071. doi:10.1158/1078-0432.CCR-17-3427.

Elective nodal irradiation attenuates the combinatorial efficacy of stereotactic radiation therapy and immunotherapy

Ariel E. Marciscano[1], **Ali Ghasemzadeh**[2], **Thomas R. Nirschl**[2], **Debebe Theodros**[2], **Christina M. Kochel**[2,3], **Brian J. Francica**[2,4], **Yuki Muroyama**[2], **Robert A. Anders**[2,5], **Andrew B. Sharabi**[6], **Esteban Velarde**[1], **Wendy Mao**[2], **Kunal R. Chaudhary**[7], **Matthew G. Chaimowitz**[8], **John Wong**[1], **Mark J. Selby**[9], **Kent B. Thudium**[9], **Alan J. Korman**[9], **David Ulmert**[10], **Daniel L.J. Thorek**[2,11], **Theodore L. DeWeese**[1,2], and **Charles G. Drake**[2,8,*]

[1]Department of Radiation Oncology & Molecular Radiation Sciences, Sidney Kimmel, Comprehensive Cancer Center, Johns Hopkins University School of Medicine, Baltimore, MD, USA 21231

[2]Department of Oncology, Sidney Kimmel Comprehensive Cancer Center, Johns Hopkins, University School of Medicine, Baltimore, MD, USA 21287

[5]Department of Pathology, Sidney Kimmel Comprehensive Cancer Center, Johns Hopkins, University School of Medicine, Baltimore, MD, USA 21287

[6]Department of Radiation Medicine and Applied Sciences, UC San Diego Moores Cancer Center, San Diego, CA, USA 92093

[7]Department of Radiation Oncology, Columbia University Medical Center, New York, New York

[8]Division of Hematology and Oncology, Herbert Irving Comprehensive Cancer Center, Columbia University Medical Center, New York, NY, USA 10032

[9]Bristol-Myers Squibb Company, Redwood City, CA, USA 94063

[10]Molecular Pharmacology Program, Memorial Sloan Kettering Cancer Center, New York, NY, USA 10065

[11]Division of Nuclear Medicine and Molecular Imaging, Department of Radiology and Radiological Science, Johns Hopkins University School of Medicine, Baltimore, MD, USA 21205

Abstract

PURPOSE—In the proper context, radiation therapy (RT) can promote anti-tumor immunity. It is unknown if elective nodal irradiation (ENI), a strategy that irradiates tumor-associated draining lymph nodes (DLN), impacts adaptive immune responses and combinatorial efficacy of RT with immune checkpoint blockade (ICB).

[*]**Corresponding Author:** Charles G. Drake, MD PhD, Columbia University Medical Center, Herbert Irving Comprehensive Cancer Center, Division of Hematology/Oncology, 177 Fort Washington Avenue, Suite 6GN-435, New York, NY 10032, Phone: 212-305-2055, Fax: 212-305-3035, cgd2139@cumc.columbia.edu.

[3]Current Address: Tizona Therapeutics, South San Francisco, CA, USA 94080

[4]Current Address: Aduro Biotech Inc., Berkeley, CA, USA 94710

Conflict of Interest Disclosure Statement: CGD is a co-inventor on patents licensed from JHU to BMS. MJS, KBT, and AJK are paid employees of BMS. JW is the inventor of the SARRP and receives royalty and consultancy reimbursement from Xstrahl.

EXPERIMENTAL DESIGN—We developed a preclinical model to compare stereotactic RT (Tumor RT) with or without ENI to examine immunological differences between RT techniques that spare or irradiate the DLN.

RESULTS—Tumor RT was associated with up-regulation of an intratumoral T-cell chemoattractant chemokine signature (CXCR3, CCR5-related) that resulted in robust infiltration of antigen-specific CD8+ effector T-cells as well as FoxP3+ regulatory T-cells (Tregs). The addition of ENI attenuated chemokine expression, restrained immune infiltration and adversely impacted survival when combined with ICB, especially with anti-CLTA4 therapy. The combination of stereotactic RT and ICB led to long-term survival in a subset of mice and was associated with favorable CD8 effector-to-Treg ratios and increased intratumoral density of antigen-specific CD8+ T-cells. While RT technique (Tumor RT vs. ENI) impacted initial tumor control and survival, the ability to reject tumor upon re-challenge was partially dependent upon the mechanism of action of ICB; as RT/anti-CTLA4 was superior to RT/anti-PD-1.

CONCLUSIONS—Our results highlight that irradiation of the DLN restrains adaptive immune responses through altered chemokine expression and CD8+ T-cell trafficking. These data have implications for combining RT and ICB, long-term survival and induction of immunological memory. Clinically, the immunomodulatory effect of the RT strategy should be considered when combining stereotactic RT with immunotherapy.

Keywords

stereotactic radiotherapy; radiation; cancer immunology; immunotherapy; immune checkpoint blockade; PD-1; CTLA-4; Treg; immune checkpoint inhibition

INTRODUCTION

Ionizing radiation is a cytotoxic therapy that primarily exerts its therapeutic effect via induction of double-stranded DNA breaks in tumor cells. Recent studies linking DNA damage with radiation-mediated immunogenicity provided mechanistic evidence that the immunomodulatory properties of radiation therapy (RT) also contribute to its therapeutic efficacy [1–3]. Within the irradiated tumor microenvironment (TME), RT initiates a cascade of molecular and cellular events leading to immunogenic cell death, upregulation of major histocompatibility complex (MHC) class I, enhanced Type I interferon (IFN) signaling and dendritic cell activation [4–7]. Ultimately, effective anti-tumor adaptive immunity requires the priming and subsequent chemokine-driven trafficking of tumor-specific CD8+ cytotoxic T-lymphocytes (CTL) into the TME to mediate tumoricidal effector functions [8–10].

The tumor-associated draining lymph node (DLN) is essential to the generation of tumor-specific CD8+ effector T-cells given that it is one of the main locations at which dendritic cells prime antigen-specific CD8+ T-cells [7,11–13]. Takeshima and colleagues observed that the DLN is indispensable for radiation-induced accumulation of antigen-specific intratumoral CTL – as DLN-deficient mice and mice with surgically ablated DLN showed a significant reduction in tumor control following RT [14]. Similarly, we demonstrated that stereotactic RT enhances cross-presentation of MHC class I-restricted tumor-associated

antigens in the DLN as the major mechanism by which RT promotes antigen-specific immune responses and synergizes with immunotherapy [15].

It is currently unknown whether irradiation of the DLN augments or restrains adaptive immune responses and impacts potential combinatorial efficacy with immune checkpoint blockade (ICB). This question carries significant clinical relevance as the strategy of elective nodal irradiation (ENI) is a commonly employed in the practice of radiation oncology - although its role is controversial or under investigation in certain cancer subtypes [16–19]. ENI involves RT delivered to the primary tumor as well as the irradiation of clinically uninvolved regional lymph nodes in the setting of a localized cancer to address potential nodal micrometastases. As technology evolved over the past decades, stereotactic RT is currently able to deliver precise and conformal high-dose radiation while either sparing or targeting the DLN, providing further rationale to explore the immunological implications of ENI.

To investigate these outstanding questions, we used the small animal radiation research platform (SARRP) and developed a preclinical model of ENI that closely models the clinical practice of image-guided stereotactic RT [20]. We evaluated two different RT strategies: i) tumor-only stereotactic RT (Tumor RT) and ii) ENI (T+LN RT) and dissected immunological differences in the tumor microenvironment (TME). We quantified the function and magnitude of antigen-specific T-cell responses to ascertain whether one of the two RT strategies confers a relative advantage when combined with immune checkpoint blockade. As a number of clinical trials are exploring the combination of stereotactic RT with immunotherapy, it will be important to understand if irradiation of the DLN modifies immunogenicity and potential synergy with immunotherapy.

MATERIALS AND METHODS

Mice and cell lines

Animal experiments were performed using female 6-8-week-old mice housed in pathogen-free facilities accredited by the American Association for the Accreditation of Laboratory Animal Care (AAALAC) under protocols approved by the Animal Care and Use Committee of the Johns Hopkins University School of Medicine (Baltimore MD). C57BL/6 wild type mice were purchased from The Jackson Laboratory (Bar Harbor ME). Adoptive T-cell transfer experiments were performed as previously described using congenically mismatched strains [21]. Recipient CD45.1 (B6-Ly5.1) mice were purchased from Charles River Laboratories (Boston MA). Donor OT-I/CD45.2/Rag$^{-/-}$ mice were bred in-house and have a transgenic T-cell receptor (TCR) that recognizes the H-2K^{b}–restricted class I epitope, ovalbumin (OVA) 257-264 [22].

MC38 colorectal carcinoma and B16/F10 melanoma cell lines were purchased from ATCC. MC38 and B16/F10 were cultured in complete (10% Fetal Bovine Serum, 1% antibiotic/anti-mycotic, 1% Sodium pyruvate and 1% MEM non-essential amino-acids) RPMI and DMEM, respectively, in a 37°C, 5% CO2 incubator. Some experiments used OVA antigen-expressing cell lines. MC38-OVA cells were a kind gift from Dr. Mark Smyth (QIMR Berghofer Medical Research Institute, Melbourne, Australia). B16-OVA cells were obtained

from the laboratory of Dr. Hyam Levitsky (Johns Hopkins University) and were cultured in RPMI complete media plus G418 (Sigma-Aldrich, St. Louis MO) for selection.

Intratumoral fluorescence tracking experiments, immunohistochemistry and immunofluorescence

For intratumoral fluorescence tracking experiments, tumor-bearing mice were injected with IRDye® 800CW PEG contrast agent (LI-COR, Lincoln NE) and serial *in vivo* near-IR imaging and image-guided surgery were performed as previously described [23]. For immunohistochemistry and immunofluorescence, tumor and DLN were fixed with 4% paraformaldehyde for 48 hours at 4°C, snap frozen, and stored at −80°C before sectioning. Hematoxylin and eosin (H&E) staining was performed by the histology core facility (Johns Hopkins University). Immunostaining for phospho-H2AX^{ser139} (pH2AX) with DAPI nuclear counterstain was performed by an automated immunofluorescence (Ventana Medical Systems, Inc.; Tucson AZ) Molecular Cytology core facility (Memorial Sloan Kettering Cancer Center). Images were acquired on inverted fluorescence phase contrast microscope (Olympus IX-71; Tokyo, Japan).

In vivo stereotactic radiation therapy experiments

Flank tumors were established by subcutaneous (s.c.) or intradermal (i.d.) implantation of 1.5×10^6 MC38 or MC38-OVA or 5×10^5 B16 cells on day 0 into wild-type C57BL/6J (or B6-Ly5.1/CD45.1 recipient mice for adoptive transfer experiments). On day 11, tumor-bearing mice received 12Gy of stereotactic RT. α-PD-1 (murine IgG1, anti-PD-1 clone 4H2) and depleting α-CTLA4 (murine IgG2a, anti-CTLA4 clone 9D9) antibodies (200μg) were a gift from Bristol-Myers Squibb (Redwood City, CA) under an institutionally approved Material Transfer Agreement (MTA). Therapeutic antibodies were administered by intraperitoneal (i.p.) treatment on days 10, 12, and 14 [24]. For time course experiments, mice were sacrificed on either day 11 (1hr after RT), 13 (48hr after RT) or 16 (120hrs after RT) as indicated. For studies focusing on therapeutic antibody administration, mice were sacrificed on day 21. Tumors and DLN were harvested and single-cell suspensions of tumor infiltrating lymphocytes (TIL) and DLN were prepared as previously described [15]. Briefly, suspensions were prepared by mechanical dissociation, followed by density gradient centrifugation on an 80%/40% Percoll (GE Healthcare, Marlborough MA) gradient. Tumor mass (g) was measured as wet tumor weight on day of sacrifice. For re-challenge experiments, long-term survivors with complete responses to RT plus ICB were implanted with 1.5×10^6 MC38-OVA on the contralateral flank six months after initial tumor s.c. implant.

Stereotactic radiation therapy

Mice with well-established ~300mm^3 tumors were irradiated with 12 Gy (3.0Gy/min) or sham non-irradiated, using the SARRP (Xstrahl, Suwanee GA) as previously described [20]. Briefly, mice were anesthetized with isoflurane and underwent CT imaging on the SARRP for image-guided localization of the tumor (10 mm collimator) and DLN (3 mm collimator) with placement of isocenter prior to irradiation of the tumor alone or the tumor and DLN. Detailed radiation dosimetry and radiation planning information is provided in Supplemental Figure 1.

Adoptive transfer experiments

Spleens and lymph nodes were harvested from OT-1/Rag$^{-/-}$ mice. Antigen-specific CD8+ OT-1 T-cells were isolated by positive selection (CD8a MicroBeads, Miltenyi Biotec, Auburn CA) and labeled with CFSE per manufacturer protocol (CellTrace™ CFSE kit, Thermo Fisher Scientific, Waltham MA). CFSE-labeled CD8+ OT-1 cells were re-suspended in 200uL PBS and transferred by retro-orbital injection (2×10^6 cells) on day 13 (48 hours after stereotactic RT) into congenic B6-Ly5.1/CD45.1 recipient tumor-bearing mice that had been implanted with 1.5×10^6 MC38-OVA cells on day 0. On day 16 (120 hours after RT, 72 hours after adoptive transfer), tumor and DLN were harvested and immune cells were isolated as above and stimulated with 2μM H-2K^b–restricted class I epitope SIINFEKL $OVA_{257–264}$ (AnaSpec, Fremont CA) in the presence of GolgiStop™ and GolgiPlug™ protein transport inhibitors (BD Biosciences, San Jose CA) for intracellular cytokine staining and then analyzed by flow cytometry. As a positive control, mice were vaccinated with an attenuated *Listeria monocytogenes* vector engineered to express OVA (LM-OVA), (Aduro Biotech, Berkeley CA) [25]. LM-OVA was diluted in PBS to 1×10^7 cfu per dose (0.1 LD_{50}), and administered by i.p. injection [21].

Flow cytometry and tetramer staining

Single-cell suspensions prepared from DLN and TIL were pre-incubated with mouse Fc Block™ purified anti-mouse CD16/CD32 (BD Biosciences, San Jose CA) for 30 minutes at 4°C. For tetramer staining, murine iTAg™ MHC Tetramer/PE H-2 K^b OVA (SIINFEKL) was purchased from MBL International (Woburn, MA) and staining performed per manufacturer instructions. For fluorochrome-conjugated antibodies, the following clones were used (purchased from BioLegend®, San Diego CA, except as noted): CD4 (GK1.5), CD8a (53-6.7), CD11b (M1/70; BD Biosciences, San Jose CA), CD44 (IM7), CD45 (30-F11), CD45.2 (104), CD62L (MEL-14), FoxP3 (FJK-16s, eBioscience, Waltham MA), IFNɣ (XMG1.2), Ly-G6/Ly-6G Gr-1 (RB6-8C5), Live/Dead™ fixable aqua dead cell stain kit (Thermo Fisher Scientific, Waltham MA), TNFα (MP6-XT22; BD Biosciences, San Jose CA). Flow cytometry was performed using a BD LSR II instrument (BD Biosciences, San Jose CA). Flow data were analyzed using FlowJo® v10 software (Treestar, Inc. Ashland OR). Gating strategies are shown in Supplemental Figure 2.

Luminex assay and ELISA

Tumors collected at specified post-treatment time points were mechanically dissociated, lysed and incubated on ice for 30 minutes with intermittent vortexing in CellLytic™ MT Cell Lysis Reagent (Sigma-Aldrich, St. Louis MO) containing Halt Protease and Phosphatase Inhibitor (Thermo Fisher Scientific, Waltham, MA) in a 1:100 ratio. Tumor lysates were assayed for raw protein concentration using a Coomassie assay (Bio-Rad, Hercules CA). Intratumoral chemokines and cytokines were quantified using the Bio-Plex Pro™ mouse chemokine panel assay (Bio-Rad, Hercules CA) and the multiplex MCYTOMAG-70K multiplex assay (EMD Millipore, Billerica MA). Luminex assays were conducted per vendor instructions. For ELISA experiments, TIL were stimulated overnight with OVA peptide and supernatants were collected and target cytokines were measuring using eBioscience™ mouse IFNγ, TNFα and IL-2 ELISA Ready-Set-Go! Kits (Thermo

Fisher Scientific, Waltham, MA). For IL-7 experiments, serum and supernatant derived from inguinal nodal lysate (ipsilateral to tumor) was collected and measured per vendor instructions using Mouse IL-7 ELISA kit (Thermo Fisher Scientific, Waltham, MA).

Venous blood collection for complete blood counts (whole blood hematology)

Serial complete blood counts with differential cell subset analysis were performed by collecting 100μL whole blood via tail vein puncture into K_2EDTA-coated BD Vacutainer® microcollection tubes (Becton, Dickinson and Company Franklin Lakes, NJ). Tubes were inverted/mixed 8-10 times, directly transported at room temperature to the core facility (Institute of Comparative Medicine at Columbia University) and analyzed using the Genesis™ veterinary hematology system (Oxford Science Inc., Oxford, CT).

Statistical Analysis

Statistical analyses were performed using GraphPad Prism 6 (GraphPad Software, La Jolla CA). Significance was calculated as described in figure legends. Results were considered statistically significant at $P \leq 0.05$(*).

RESULTS

Image-guided stereotactic elective nodal irradiation (ENI) accurately targets tumor-associated draining lymph nodes (DLN)

We first developed a model to quantify immunological differences between two RT strategies: (1) stereotactic RT delivered to the tumor-only (Tumor RT) and (2) stereotactic RT delivered to the tumor and the tumor-associated DLN (T+LN RT). To identify the tumor-associated DLN, we performed intratumoral injection of a fluorescent dye (IRDye® 800CW PEG contrast agent) in C57BL/6J mice implanted with B16 melanoma or MC38 colorectal carcinoma flank tumors. Serial fluorescent imaging was performed after intratumoral administration; accumulation of fluorescence within the ipsilateral inguinal DLN was noted after 1 hour (Figure 1A–1B). Fluorescence-guided surgery confirmed that the majority of the dye had trafficked from the tumor into the ipsilateral inguinal node, supporting that particular node as the predominant tumor-associated DLN in these models (Figure 1C). In subsequent experiments, cone-beam CT imaging using the SARRP reliably visualized the inguinal fat pad - allowing for delivery of image-guided stereotactic RT to the tumor-associated DLN as a model for ENI (Figure 1C, Figure S1).

To validate the ability of SARRP-based RT to accurately target or spare the DLN, we assessed induction of phospho-H2AX (pH2AX) nuclear foci as a surrogate for radiation-induced DNA double-stranded breaks [26]. Tumor and DLN were harvested from irradiated mice 1 hour after 12Gy x1 (or sham RT), delivered stereotactically. Tumor RT demonstrated clear induction of pH2AX foci in the tumor and an absence of pH2AX foci in the DLN while T+LN RT demonstrated induction of pH2AX foci in both the tumor and DLN, verifying targeted delivery of stereotactic RT (Figure 1D). To assess whether the DLN were involved with tumor, a board-certified surgical pathologist (RAA) confirmed the absence of metastatic disease in the tumor-associated DLN of untreated mice on day 14 (Figure 1E); this was critical given that ENI is a strategy used in clinically localized tumors that do not

have evidence of locoregional metastases [16–18]. In subsequent studies, stereotactic RT was delivered on day 11 (tumor volume ~200-300mm^3), thus animals were unlikely to harbor gross nodal metastases at the time of treatment.

Elective nodal irradiation (ENI) decreases tumor-infiltrating immune cell density relative to Tumor-only stereotactic RT

We next performed a series of experiments to qualitatively and quantitatively test for differences in tumor-infiltrating immune cell phenotype between Tumor RT and T+LN RT. Relative to untreated mice (control), Tumor RT significantly ($P<0.001$) enhanced the intratumoral density of effector (CD44+ CD62L-) CD8+ T-cells (CD8+ effector, Figure 2A, left panel). Tumor RT also significantly increased ($P<0.001$) the absolute number (per gram tumor) of intratumoral FoxP3+ CD4+ T-cells (Tregs) and CD11b+ Gr-1^{hi} myeloid cells (Figure 2B–2C, left panel). In sum, the addition of RT to the DLN (T+LN RT) was associated with a statistically significant decrease ($P<0.001$) in the intratumoral density of all three immune cell subsets (CD8 effectors, Tregs and CD11b+Gr-1^{hi} myeloid cells) as compared with Tumor RT (Figure 2A–2C, left panel).

Normalized to the control group, there were significant ($P<0.001$) 12.5-fold and 4.0-fold increases in intratumoral density of CD8 effectors and Tregs in the Tumor RT group, respectively (Figure 2D). T+LN RT was not associated with a significant modulation of either tumor-infiltrating subset with a 2.1-fold increase in CD8+ effectors and no change in Tregs. Nevertheless, both Tumor RT and T+LN RT increased the CD8 effector-to-Treg ratio, relative to non-irradiated controls (Figure 2D). When comparing RT strategies, the CD8 effector-to-Treg ratio was significantly greater with Tumor RT ($P=0.001$, Tumor RT 8.8 vs. T+LN RT 6.3). Taken together, these findings show that irradiation of the DLN has a significant impact on immune infiltration of the TME and that multiple immunological differences exist between Tumor RT as compared to T+LN RT.

Tumor RT and T+LN RT have distinct radiation-induced intratumoral chemokine expression and CD8+ T-cell trafficking patterns

We next sought to elucidate the mechanisms underlying the differences in intratumoral immune infiltration between RT strategies. Time course experiments demonstrated a significant ($P<0.001$) increase in the absolute number of viable CD45+ cells within the tumor-associated DLN 48 hours after Tumor RT (Figure S3); this was not observed in the control or T+LN RT groups. Further dissection of the CD45+ population demonstrated that this was predominantly driven by an increase in the total number of CD8+ T-cells at the 48-hour time point, i.e. we observed a 2.5-fold increase relative to the untreated control and 2.2-fold increase relative to the T+LN RT group (Figure 3A). At these post-RT time points, Luminex® multiplex immunoassay of tumor lysate demonstrated a distinct pattern of upregulation of chemokines associated with T-cell chemoattraction; this was observed predominantly in the Tumor RT group (Figure 3B). Specifically, 48 hours after Tumor RT there was a significant upregulation of CXCR3 and CCR5-associated chemokines (i.e. CXCL10, CCL3, CCL5) which have been shown to be important for recruitment of antigen-specific CD8+ effector T-cells into the tumor microenvironment [9–10,27–29]. This upregulation of intratumoral chemokines was attenuated in T+LN RT-treated mice.

Untreated (control) tumors demonstrated increased expression of IL-1β and IL-6 over time which has been associated with poor prognosis, tumor progression and immunosuppression [30–32]. Complete quantitative data are provided in Figure S3. Collectively, these data suggest that ENI attenuates RT-mediated chemokine expression in the TME; this decreased chemokine expression may explain reduced CD8 effector infiltration in the T+LN group.

Radiation-mediated tumor infiltration with functional antigen-specific CD8+ T-cells is restrained by ENI

Given that radiation enhances cross-priming of antigen-specific CD8+ effector T-cells primarily within the tumor-associated DLN [14–15], we queried whether T + LN RT (ENI) alters the effector function of antigen-specific T-cells in the tumor microenvironment. For these experiments, we used MC38-OVA and B16-OVA tumors - with the notion that in this system, OVA models a mutation-associated neo-antigen (MANA) to which high-affinity T-cells may exist [33]. To quantify antigen-specific T-cell responses, we performed adoptive transfer experiments in which naïve CFSE-labeled OVA-specific CD8+ T-cells (OT-1) were transferred into host mice bearing OVA-expressing tumors 48 hours after stereotactic RT. For a positive control we transferred cells to non-irradiated, non-tumor bearing mice and vaccinated recipients with LM-OVA, this resulted in > 90% T cell division with > 50% of divided cells positive for IFNγ (supplemental Figure S3C).

Consistent with the chemokine data in Figure 3, we found that Tumor RT versus T+LN RT resulted in significant differences in immunological parameters in the TME. The absolute number (per gram tumor) of effector cytokine-producing, dividing OT-1 cells was significantly greater ($P<0.001$) in the Tumor RT group (Figure 4A, left panels). Endogenous (CD45.2 negative) CD8 T-cells (Figure 4A, center panels) showed a similar pattern. These findings were supported by ELISA data (Figure 4A, right panels) showing that the concentration of IFNγ and TNFα in the supernatant collected from OVA-stimulated TIL was significantly increased in the Tumor RT group relative to both control ($P<0.001$) and T +LN RT ($P<0.001$). Corroborating these results with endogenous antigen-specific T-cells, H-2kb OVA (SIINFEKL) tetramer staining showed that Tumor RT significantly enhanced the absolute number of tumor-infiltrating tetramer-positive CD8+ effectors as compared with T+LN RT ($P<0.001$) (Figure 4B, middle panel). As expected, the tumor-infiltrating CD8+ effector population was largely comprised of tetramer-negative cells (Figure 4B, right panel). Further, endogenous effector (non-OT-1) IFNγ+/TNFα+ CD8+ T-cells were significantly enriched in the Tumor RT group, supporting that non-OVA specific intratumoral T-cells were also potentially functional (Figure 4A, middle panel). Taken together, these data show that RT to the tumor alone (as compared to T+LN RT) was associated with increased intratumoral infiltration of both antigen-specific as well as additional effector T-cells.

Turning to the DLN, we found that there were no significant differences in OT-1 division in the DLN between Tumor RT and T+LN RT (supplemental Figure S3C). However, the proportion of effector cytokine-producing divided OT-1 cells was significantly decreased (IFNγ+, $P<0.05$; TNFα+, $P<0.001$) in the DLN of mice treated with Tumor RT alone as compared to T + LN RT (Figure 4C). Thus, the findings in the DLN suggested that T+LN

RT may not limit the initial priming of antigen-specific T-cells. However, it is notable that this RT strategy (ENI) was associated with a significant reduction in the intratumoral accumulation of antigen-specific functional CD8 effectors. This contrasts the finding of increased CD8+ T-cell infiltration into the TME associated with Tumor RT alone (Figures 4A and 4B) and further supports the concept that RT target/site alters T-cell migration and effector function.

ENI attenuates combinatorial efficacy between radiation and immunotherapy

Since significant immunological differences were observed between Tumor RT and T+LN RT, we next explored whether these differences would be reflected in a therapeutic model of stereotactic RT – either alone or in combination with immune checkpoint blockade (Figure 5A). For these studies, we used a blocking PD-1 antibody (clone 4H2) and an IgG2a isotype CTLA4 antibody; the latter reagent partially depletes Tregs in the TME reflecting the IgG1 isotype of the FDA-approved anti-CTLA4 agent (ipilimumab) [24]. While Tumor RT and T+LN RT each increased median survival compared with untreated controls (isotype), neither approach resulted in complete tumor regression or long-term survival. Tumor RT prolonged median survival relative to T+LN RT ($P<0.001$; 41 vs. 25 days), however, all tumors eventually recurred (Figure 5B-D). When combined with PD-1 blockade, both RT strategies conferred a survival advantage relative to αPD-1 monotherapy, with a complete response rate of 29% and 31% in Tumor RT/αPD-1 and T+LN RT/ αPD-1, respectively. However, there were no differences in median survival or response rate between combination therapies with RT+αPD-1. In the context of concurrent αCTLA4, ENI adversely impacted survival [24]. Tumor RT/αCTLA4 yielded a complete response rate of 86% and median survival had not been reached by day 90. In the T+LN RT/αCTLA4 group, irradiation of the tumor-associated DLN significantly reduced median survival (62 days) and complete response rate (43%) relative to Tumor RT/αCTLA4 ($P<0.001$) – similar to the response rate observed for both RT+αPD-1 combinations (Figure 5D). Notably, in this established MC38-OVA model (Day 11), αPD-1 monotherapy was largely ineffective and yielded no complete responses [34]. Conversely, αCTLA4 monotherapy induced complete tumor regression in 29% of mice. Despite differences in efficacy between αPD-1 and αCTLA4, a negative association of ENI upon survival was evident when comparing T+LN RT versus Tumor RT as well as T+LN RT/αCTLA4 vs. Tumor RT/αCTLA4.

Favorable modulation of intratumoral CD8 effector-to-Treg ratio is associated with long-term survival

To quantify immunological parameters associated with response to combination therapy with stereotactic RT and ICB, we performed immunophenotyping to evaluate differences in intratumoral immune modulation between treatment groups. It should be noted that these studies focused on well-established tumors (Day 11, ~ $300mm^3$); as above, PD-1 blockade is generally ineffective as a monotherapy for late-stage MC38 tumors [34]. Broadly, our findings suggested that the absolute number (per gram tumor) of intratumoral CD8 effectors and as well as a favorable CD8 effector-to-Treg ratio correlate with a survival benefit. The Tumor RT/αCTLA4 group, which yielded the greatest number of complete responses and longest median survival, was found to have a significantly elevated CD8 effector-to-Treg ratio (110.1); this was substantially greater than all other treatment groups (Figure 6C,

bottom panel). Similar to our prior findings (see Figure 2), Tumor RT was associated with a significant increase in the intratumoral density of CD8 effectors and Tregs relative to control and to T+LN RT (Figure 6C, left upper/middle panel; all P<0.001). In the context of ICB with either αPD-1 or αCLTA4, Tumor RT significantly enhanced CD8 effector infiltration relative to either ICB monotherapy (all P<0.001) and also enhanced CD8 effector infiltration relative to T+LN RT when combined with αPD-1 or αCLTA4 (all P<0.001), respectively (Figure 6C, upper panel). PD-1 blockade appeared to have a modest impact on the Treg subsets in this model (Figure 6C, middle/central panel). However, αCTLA4 as a monotherapy or in combination with Tumor RT decreased intratumoral Tregs [24,35–36]. In contrast, when T+LN RT was combined with αCTLA4, there was a significant increase in intratumoral Tregs, relative to both Tumor RT and control (both P<0.001, Figure 6C, right middle panel). Taken together, the ability of αCTLA4 IgG2a to enhance CD8 effectors and reduce Tregs promoted the pro-immunogenic effects of Tumor RT and limited its immunosuppressive effects, thereby favorably increasing the CD8 effector-to-Treg ratio (Figure 6C bottom panel).

Improved resistance to re-challenge in animals treated with RT + αCTLA4

We next set out to assess the longer-term outcome of RT technique in the presence or absence of ICB. On day 21 post-tumor inoculation (day 10 post-RT), H-2kb OVA tetramer analysis of tumors harvested after treatment with Tumor RT/αCTLA4 demonstrated the most robust infiltration of OVA-specific CD8+ effectors. Indeed, the intratumoral density of antigen-specific CD8+ effectors with this pairing was 3-fold greater than any other treatment group (Figure 7A). With regards to effector cytokine production in response to OVA peptide stimulation, intratumoral IFNɣ expression most strongly correlated with the density of antigen-specific immune cells as well as survival (Figure 7B) [37].

Finally, to functionally ascertain whether the development of a protective memory response was influenced by treatment type, we re-challenged surviving mice a full six months (180 days) after initial tumor implantation. For these studies, the only animals that achieved long-lasting complete responses were those treated with combined stereotactic RT and ICB. As mentioned, > 85% of mice treated with Tumor RT/αCTLA4 achieved complete responses/ long-term survival while long-term survival with other combination RT/immunotherapy groups ranged 28 - 43% (Figure 5D) – therefore the initial combination RT/immunotherapy strategy influenced survival and thus the ability to be rechallenged. When stratifying the subset of long-term survivors by ICB type, mice previously treated with a αCTLA4-based combination regimen (Tumor RT/αCTLA4 and T+LN RT/αCTLA4) were more resistant to re-challenge (Figure 7C). Specifically, 100% of the prior αCTLA4-treated group survived rechallenge, while by comparison 50% of prior αPD1-treated animals survived rechallenge (Figure 7C). Among the αPD1-treated mice that were unable to clear tumor, there was a significant tumor growth delay (P=0.003, median survival 51 vs. 22 days) relative to tumor implantation in naïve host animals (Figure 7C). When stratifying by initial RT strategy (Tumor RT vs. T+LN RT), there was no appreciable impact on subsequent tumor rejection in the context of rechallenge (Figure 7C).

DISCUSSION

The optimal delivery of stereotactic RT to promote immunogenicity remains an open area of investigation. Specifically, it is currently unknown whether irradiating the tumor-associated DLN modulates adaptive immunity and therefore the potential of RT to effectively synergize with immunotherapy. Here, we developed a preclinical model of elective nodal irradiation (ENI), acknowledging that we verified the absence of nodal micrometastases by histopathology. We used this model to evaluate the immunological implications of stereotactic RT strategies that either target or spare the tumor-associated DLN. One important feature of these studies is our use of the SARRP, which allowed for these preclinical *in vivo* RT studies to model the delivery of image-guided RT in clinical practice. To further enhance the clinical relevance and rigor of our model, fluorescence-guided surgery performed after intratumoral injection of a fluorescent dye identified the inguinal lymph node as the predominant tumor-associated DLN (Figure 1A). This is akin to lymphatic mapping which is commonplace in breast cancer or melanoma as intratumoral radiotracer and/or dye are used to identify the sentinel DLN.

We found that Tumor RT and ENI (T+LN RT) yielded distinct intratumoral chemokine expression profiles which were associated with significant differences in immune infiltration of the TME. Consistent with the existing literature, Tumor RT was associated with significant upregulation of CXCL10, CXCL16 and other CCR5-related chemokines (Figures 3B, S3B). RT-mediated type I/II IFN signaling appears to be important for increased intratumoral CXCL10 levels (interferon-ɣ-induced protein 10, IP-10) which correlates with intratumoral accumulation of CD8+ T-cells [27,29]. It was recently demonstrated that the CXCL10/CXCR3 chemokine-chemokine receptor axis is required for intratumoral CD8 effector T-cell homing from the DLN and periphery [28]. Matsumura and colleagues demonstrated the RT-induced CXCL16 secretion from irradiated breast cancer cells specifically recruit CD8+ effector T-cells expressing the cognate CXCR6 chemokine receptor [10]. Additionally, enhanced intratumoral expression of CXCL10 and CCL5 was observed following tumor irradiation in a Panc02-SIY pancreatic tumor model [38]. Taken together, our findings suggest that Tumor RT induces an intratumoral T-cell chemoattractant chemokine signature that promotes robust infiltration of functional CD8+ effector T-cells.

Our most striking finding was that RT-mediated chemokine expression was attenuated by ENI (T+LN RT), leading to impaired trafficking of CD8+ T-cells into the TME and, ultimately, decreased survival in our therapeutic model (Figures 1A, 4D). Given those findings, we also considered a potential contribution of direct lymphotoxic effects upon the irradiated DLN. We noted a modest decline in live CD45+ cells within the irradiated DLN (Figure 3A, S3A). Systemically, we noted a modest decline in circulating lymphocytes among irradiated mice but did not observe significant differences in peripheral lymphocyte counts between Tumor RT and T+LN RT nor indication of severe treatment-related lymphopenia (Figure S4A). However, a contributory effect of lymphodepletion cannot be entirely excluded in this model. Arguing against this possibility, T+LN RT was associated with the highest proportion of dividing antigen-specific cells and the greatest number of IFNɣ+ and TNFα+ antigen-specific CD8+ T-cells within the tumor-associated DLN (Figure 4C). These data suggest that there was a pool of functional antigen-specific CD8+ T-cells

present within the DLN that ultimately did not traffic into the TME when the DLN was irradiated (Figure 3A, 4A-B). In support of this finding, Mikucki and colleagues demonstrated that adoptively transferred CXCR3$^{-/-}$ deficient OT-1 cells have limited intratumoral localization capacity relative to wildtype OT-1 counterparts despite having equivalent cytotoxic activity and effector cytokine (IFNγ and granzyme B) production [28]. Taken together, our findings suggest that the irradiation of the DLN disrupts the chemokine-driven orchestration of effector T-cell recruitment into the TME. These novel observations regarding ENI improve our understanding of RT-mediated adaptive anti-tumor immune responses and have implications for the combination of RT and ICB in the clinic.

While Tumor RT promotes CD8+ effector infiltration it can also increase intratumoral Tregs (Figure 2B) and CD11b+ Gr-1^{hi} myeloid cells (Figure 2C) which can restrain CD8+ effector functions [39,40]. Our group recently demonstrated that stereotactic Tumor RT not only increases Treg intratumoral density but also enhances their suppressive function [41]. Thus, the opposing immuno-stimulatory and tolerogenic effects of RT may provide insight into potential mechanisms to optimize synergy with immunotherapy [42]. An elevated CD8 effector-to-Treg ratio has been associated with favorable prognosis and survival across multiple cancer subtypes and therefore we used this as a surrogate of favorable immune modulation in our study [15,43,44].

We found that increased CD8 effector intratumoral density and an increased CD8 effector-to-Treg ratio were associated with survival in our therapeutic model of stereotactic RT and ICB (Figure 5). Among all treatment groups, Tumor RT/αCTLA4 was associated with the greatest response rate and the most favorable long-term survival outcomes (Figure 5). We observed that the CD8 effector-to-Treg ratio was significantly increased with Tumor RT/αCTLA4 than any other regimen and therefore interrogated potential mechanisms of synergy (Figure 6E). Anti-CTLA4-mediated Treg depletion appeared to be potentially important for combinatorial efficacy as this negated deleterious intratumoral Treg accumulation. Young and colleagues also noted a profound impact of αCTLA4-mediated Treg depletion when combined with hypofractionated RT [45]. These investigators reported that combinatorial efficacy was dependent on timing of anti-CTLA4 administration as well as FcγR-dependent Treg depletion which appears to dictate the therapeutic activity of αCTLA-4 IgG2a across several preclinical murine models [24,35–36]. We independently confirmed that αCTLA4 IgG2a appears to deplete intratumoral Tregs more efficiently than αCTLA4 IgG2b and this effect was mostly limited to intratumoral Tregs (Figure S5C, S5D).

Perhaps the most important observation from our studies is that ENI attenuated the synergy of stereotactic RT and αCTLA4 IgG2a. Depleting anti-CTLA4 antibodies have been demonstrated to possess dual function, potentially by promoting T-cell activation within the DLN during the priming phase and depleting intratumoral Tregs during the effector phase [24,35–36]. Our findings suggest a potentially important tolerogenic effect of ENI upon the DLN that was amplified by concurrent αCTLA4 and which promoted Treg expansion [24,35]. Curiously, αCTLA4 IgG2a combined with ENI increased the density of intratumoral Tregs which ultimately lead to a decrease in the CD8 effector-to-Treg ratio and decrement in survival, relative to Tumor RT/αCTLA4 (Figure 5, 6D, 6E). ENI was also found to directly dampen antigen-specific anti-tumor immune responses. Indeed, our

adoptive transfer experiments and tetramer staining revealed a significant reduction in the intratumoral density of antigen-specific functional CD8 effectors in the T+LN RT group, relative to Tumor RT (Figure 4B). This is further corroborated by the finding that T+LN RT/αCTLA4-treated tumors were significantly less infiltrated with antigen-specific CTLs compared with Tumor RT/αCTLA4-treated counterparts. These data support the conclusion that the combinatorial effects of Tumor RT/αCTLA4 in our study results from RT-mediated antigen-specific adaptive immunity (Figure 7A, 7B).

Relatively few studies to date have explored whether the combination of stereotactic RT and ICB impacts antigen-specific immunological memory. The observation that initial treatment with RT/αCTLA4 combination regimens did confer an advantage relative to RT/αPD-1-based therapies in this model system is provocative and hypothesis-generating (Figure 7C). While clinical data in the metastatic setting suggest that PD-1 blockade has improved efficacy and a favorable toxicity profile relative to CTLA4 blockade, it remains unknown which ICB is a more synergistic partner for stereotactic RT. Encouragingly, recent work by Twyman-Saint Victor et al. has demonstrated that αPD-L1, αCTLA4 and hypofractionated RT can each cooperate via non-redundant mechanisms to boost anti-tumor immunity [46]. Consistent with our findings, De La Maza et al. recently showed that combination therapy with RT/αCTLA4 was superior to RT/αPD-1 in a neoadjuvant hypofractionated RT preclinical mesothelioma model [47].

In summary, our data suggest that ENI dampens adaptive immunity through perturbation of chemokine signaling leading to reduced antigen-specific immune infiltration. Further, improved survival was achieved through the combination of Tumor RT that avoids the tumor-associated DLN and ICB (particularly RT/αCTLA4). Mechanistically, this combination augments the CD8 effector-to-Treg ratio and intratumoral density of antigen-specific functional CD8 effectors.

There are inherent limitations to these preclinical studies that caution broad application of these principles to clinical practice without additional investigation. Our studies were designed to explicitly evaluate localized, non-metastatic tumors without locoregional nodal dissemination and cannot be generalized to more advanced stages of disease. Given the complex interplay between RT and immunotherapy, disease-specific, TME-intrinsic and patient-specific factors should be taken into consideration when deciding to electively irradiate or spare the regional lymph nodes. While the mechanism of action of immunotherapy was an important determinant of response in this model, additional variables including the relative timing/sequencing of therapies, dose-fractionation schedules were not evaluated and may yield additional insight into the immunological implications of ENI. As numerous clinical trials are underway that are actively exploring the interaction of dose/fractionation and sequencing of RT and immunotherapy, our data highlight the importance of the RT target and RT strategy. As such, this work provides preclinical data suggesting that irradiation of the DLN should potentially be avoided in order to promote combinatorial efficacy between RT and immunotherapy.

Supplementary Material

Refer to Web version on PubMed Central for supplementary material.

Acknowledgments

We would like to thank the Experimental Irradiator Core within the Johns Hopkins Sidney Kimmel Comprehensive Cancer Center, Dr. Robert A. Anders for immunopathology expertise, the Flow Cytometry Core (Julie Nauroth) and Immune Monitoring Core (Christopher Thoburn) within the Bloomberg~Kimmel Institute for Cancer Immunotherapy as well as members of Dr. Daniel L.J. Thorek's laboratory and Dr. Jonathan D. Powell's laboratory.

Financial Support: AEM was supported by an American Society for Radiation Oncology (ASTRO) Residents/ Fellows in Radiation Oncology Research Seed Grant award number 120506. AG was supported by the NIH under award number T32GM007309. CGD was supported by NIH Grants R01CA154555 and P30CA006973, the Patrick C. Walsh Prostate Cancer Research Fund, the One-in-Six Foundation, the Prostate Cancer Foundation, Melanoma Research Alliance and the BMS International Immunotherapy Oncology Network (IIoN).

References

1. Vanpouille-Box C, Alard A, Aryankalayil MJ, et al. DNA exonuclease Trex1 regulates radiotherapy-induced tumour immunogenicity. Nat Commun. 2017; 8:15618. [PubMed: 28598415]
2. Deng L, Liang H, Xu M, et al. STING-dependent cytosolic DNA sensing promotes radiation-induced type I interferon-dependent antitumor immunity in immunogenic tumors. Immunity. 2014; 41(5):843–852. [PubMed: 25517616]
3. Harding SM, Benci JL, Irianto J, Discher DE, Minn AJ, Greenberg RA. Mitotic progression following DNA damage enables pattern recognition within micronuclei. Nature. 2017; 548(7668): 466–470. [PubMed: 28759889]
4. Golden EB, Frances D, Pellicciotta I, Demaria S, Helen Barcellos-Hoff M, Formenti SC. Radiation fosters dose-dependent and chemotherapy-induced immunogenic cell death. Oncoimmunology. 2014; 3:e28518. [PubMed: 25071979]
5. Reits EA, Hodge JW, Herberts CA, et al. Radiation modulates the peptide repertoire, enhances MHC class I expression, and induces successful antitumor immunotherapy. J Exp Med. 2006; 203(5): 1259–1271. [PubMed: 16636135]
6. Burnette BC, Liang H, Lee Y, et al. The efficacy of radiotherapy relies upon induction of type i interferon-dependent innate and adaptive immunity. Cancer Res. 2011; 71(7):2488–2496. [PubMed: 21300764]
7. Fuertes MB, Kacha AK, Kline J, et al. Host type I IFN signals are required for antitumor CD8+ T cell responses through CD8{alpha}+ dendritic cells. J Exp Med. 2011; 208(10):2005–2016. [PubMed: 21930765]
8. Dovedi SJ, Lipowska-Bhalla G, Beers SA, et al. Antitumor efficacy of radiation plus immunotherapy depends upon dendritic cell activation of effector CD8+ T cells. Cancer Immunol Res. 2016; 4(7):621–630. [PubMed: 27241845]
9. Lugade AA, Moran JP, Gerber SA, Rose RC, Frelinger JG, Lord EM. Local radiation therapy of B16 melanoma tumors increases the generation of tumor antigen-specific effector cells that traffic to the tumor. J Immunol. 2005; 174(12):7516–7523. [PubMed: 15944250]
10. Matsumura S, Wang B, Kawashima N, et al. Radiation-induced CXCL16 release by breast cancer cells attracts effector T cells. J Immunol. 2008; 181(5):3099–3107. [PubMed: 18713980]
11. Diamond MS, Kinder M, Matsushita H, et al. Type I interferon is selectively required by dendritic cells for immune rejection of tumors. J Exp Med. 2011; 208(10):1989–2003. [PubMed: 21930769]
12. Spranger S, Dai D, Horton B, Gajewski TF. Tumor-residing Batf3 dendritic cells are required for effector T cell trafficking and adoptive T cell therapy. Cancer Cell. 2017; 31(5):723.e4.
13. Liao YP, Wang CC, Butterfield LH, et al. Ionizing radiation affects human MART-1 melanoma antigen processing and presentation by dendritic cells. J Immunol. 2004; 173(4):2462–2469. [PubMed: 15294960]

14. Takeshima T, Chamoto K, Wakita D, et al. Local radiation therapy inhibits tumor growth through the generation of tumor-specific CTL: Its potentiation by combination with Th1 cell therapy. Cancer Res. 2010; 70(7):2697–2706. [PubMed: 20215523]
15. Sharabi AB, Nirschl CJ, Kochel CM, et al. Stereotactic radiation therapy augments antigen-specific PD-1-mediated antitumor immune responses via cross-presentation of tumor antigen. Cancer Immunol Res. 2015; 3(4):345–355. [PubMed: 25527358]
16. Amini A, Jones BL, Yeh N, Rusthoven CG, Armstrong H, Kavanagh BD. Survival outcomes of whole-pelvic versus prostate-only radiation therapy for high-risk prostate cancer patients with use of the national cancer data base. Int J Radiat Oncol Biol Phys. 2015; 93(5):1052–1063. [PubMed: 26581142]
17. Blanchard P, Faivre L, Lesaunier F, et al. Outcome according to elective pelvic radiation therapy in patients with high-risk localized prostate cancer: A secondary analysis of the GETUG 12 phase 3 randomized trial. Int J Radiat Oncol Biol Phys. 2016; 94(1):85–92. [PubMed: 26576711]
18. Rwigema JC, Chen AM, Wang PC, Lee JM, Garon E, Lee P. Incidental mediastinal dose does not explain low mediastinal node recurrence rates in patients with early-stage NSCLC treated with stereotactic body radiotherapy. Clin Lung Cancer. 2014; 15(4):287–293. [PubMed: 24594401]
19. Wild AT, Herman JM, Dholakia AS, et al. Lymphocyte-sparing effect of stereotactic body radiation therapy in patients with unresectable pancreatic cancer. Int J Radiat Oncol Biol Phys. 2016; 94(3): 571–579. [PubMed: 26867885]
20. Wong J, Armour E, Kazanzides P, et al. High-resolution, small animal radiation research platform with x-ray tomographic guidance capabilities. Int J Radiat Oncol Biol Phys. 2008; 71(5):1591–1599. [PubMed: 18640502]
21. Jackson CM, Kochel CM, Nirschl CJ, et al. Systemic tolerance mediated by melanoma brain tumors is reversible by radiotherapy and vaccination. Clin Cancer Res. 2016; 22(5):1161–1172. [PubMed: 26490306]
22. Li M, Davey GM, Sutherland RM, et al. Cell-associated ovalbumin is cross-presented much more efficiently than soluble ovalbumin in vivo. J Immunol. 2001; 166(10):6099–6103. [PubMed: 11342628]
23. Okusanya OT, Madajewski B, Segal E, et al. Small portable interchangeable imager of fluorescence for fluorescence guided surgery and research. Technol Cancer Res Treat. 2015; 14(2): 213–220. DOI: 10.7785/tcrt.2012.500400 [PubMed: 24354756]
24. Selby MJ, Engelhardt JJ, Quigley M, et al. Anti-CTLA-4 antibodies of IgG2a isotype enhance antitumor activity through reduction of intratumoral regulatory T cells. Cancer Immunol Res. 2013; 1(1):32–42. [PubMed: 24777248]
25. Lauer P, Chow MY, Loessner MJ, Portnoy DA, Calendar R. Construction, characterization, and use of two listeria monocytogenes site-specific phage integration vectors. J Bacteriol. 2002; 184(15): 4177–4186. [PubMed: 12107135]
26. Rogakou EP, Pilch DR, Orr AH, Ivanova VS, Bonner WM. DNA double-stranded breaks induce histone H2AX phosphorylation on serine 139. J Biol Chem. 1998; 273(10):5858–5868. [PubMed: 9488723]
27. Lim JY, Gerber SA, Murphy SP, Lord EM. Type I interferons induced by radiation therapy mediate recruitment and effector function of CD8(+) T cells. Cancer Immunol Immunother. 2014; 63(3): 259–271. [PubMed: 24357146]
28. Mikucki ME, Fisher DT, Matsuzaki J, et al. Non-redundant requirement for CXCR3 signalling during tumoricidal T-cell trafficking across tumour vascular checkpoints. Nat Commun. 2015; 6:7458. [PubMed: 26109379]
29. Lugade AA, Sorensen EW, Gerber SA, Moran JP, Frelinger JG, Lord EM. Radiation-induced IFN-gamma production within the tumor microenvironment influences antitumor immunity. J Immunol. 2008; 180(5):3132–3139. [PubMed: 18292536]
30. Song X, Krelin Y, Dvorkin T, et al. CD11b+/gr-1+ immature myeloid cells mediate suppression of T cells in mice bearing tumors of IL-1beta-secreting cells. J Immunol. 2005; 175(12):8200–8208. [PubMed: 16339559]

31. Mitsunaga S, Ikeda M, Shimizu S, et al. Serum levels of IL-6 and IL-1beta can predict the efficacy of gemcitabine in patients with advanced pancreatic cancer. Br J Cancer. 2013; 108(10):2063–2069. [PubMed: 23591198]
32. Narita Y, Kitamura H, Wakita D, et al. The key role of IL-6-arginase cascade for inducing dendritic cell-dependent CD4(+) T cell dysfunction in tumor-bearing mice. J Immunol. 2013; 190(2):812–820. [PubMed: 23248265]
33. Skora AD, Douglass J, Hwang MS, et al. Generation of MANAbodies specific to HLA-restricted epitopes encoded by somatically mutated genes. Proc Natl Acad Sci U S A. 2015; 112(32):9967–9972. DOI: 10.1073/pnas.1511996112 [PubMed: 26216968]
34. Allard B, Pommey S, Smyth MJ, Stagg J. Targeting CD73 enhances the antitumor activity of anti-PD-1 and anti-CTLA-4 mAbs. Clin Cancer Res. 2013; 19(20):5626–5635. DOI: 10.1158/1078-0432.CCR-13-0545 [PubMed: 23983257]
35. Peggs KS, Quezada SA, Chambers CA, Korman AJ, Allison JP. Blockade of CTLA-4 on both effector and regulatory T cell compartments contributes to the antitumor activity of anti-CTLA-4 antibodies. J Exp Med. 2009; 206(8):1717–1725. [PubMed: 19581407]
36. Simpson TR, Li F, Montalvo-Ortiz W, et al. Fc-dependent depletion of tumor-infiltrating regulatory T cells co-defines the efficacy of anti-CTLA-4 therapy against melanoma. J Exp Med. 2013; 210(9):1695–1710. [PubMed: 23897981]
37. Gerber SA, Sedlacek AL, Cron KR, Murphy SP, Frelinger JG, Lord EM. IFN-gamma mediates the antitumor effects of radiation therapy in a murine colon tumor. Am J Pathol. 2013; 182(6):2345–2354. [PubMed: 23583648]
38. Zheng W, Skowron KB, Namm JP, et al. Combination of radiotherapy and vaccination overcomes checkpoint blockade resistance. Oncotarget. 2016; 7(28):43039–43051. [PubMed: 27343548]
39. Kachikwu EL, Iwamoto KS, Liao YP, et al. Radiation enhances regulatory T cell representation. Int J Radiat Oncol Biol Phys. 2011; 81(4):1128–1135. [PubMed: 21093169]
40. Xu J, Escamilla J, Mok S, et al. CSF1R signaling blockade stanches tumor-infiltrating myeloid cells and improves the efficacy of radiotherapy in prostate cancer. Cancer Res. 2013; 73(9):2782–2794. [PubMed: 23418320]
41. Muroyama Y, Nirschl TR, Kochel CM, et al. Stereotactic radiotherapy increases functionally suppressive regulatory T cells in the tumor microenvironment. Cancer Immunol Res. 2017; 5(11): 992–1004. DOI: 10.1158/2326-6066.CIR-17-0040 [PubMed: 28970196]
42. Barker HE, Paget JT, Khan AA, Harrington KJ. The tumour microenvironment after radiotherapy: Mechanisms of resistance and recurrence. Nat Rev Cancer. 2015; 15(7):409–425. [PubMed: 26105538]
43. Sato E, Olson SH, Ahn J, et al. Intraepithelial CD8+ tumor-infiltrating lymphocytes and a high CD8+/regulatory T cell ratio are associated with favorable prognosis in ovarian cancer. Proc Natl Acad Sci U S A. 2005; 102(51):18538–18543. [PubMed: 16344461]
44. Zeng J, See AP, Phallen J, et al. Anti-PD-1 blockade and stereotactic radiation produce long-term survival in mice with intracranial gliomas. Int J Radiat Oncol Biol Phys. 2013; 86(2):343–349. [PubMed: 23462419]
45. Young KH, Baird JR, Savage T, et al. Optimizing timing of immunotherapy improves control of tumors by hypofractionated radiation therapy. PLoS One. 2016; 11(6):e0157164. [PubMed: 27281029]
46. Twyman-Saint Victor C, Rech AJ, Maity A, et al. Radiation and dual checkpoint blockade activate non-redundant immune mechanisms in cancer. Nature. 2015; 520(7547):373–377. [PubMed: 25754329]
47. De La Maza L, Wu M, Wu L, et al. In situ vaccination after accelerated hypofractionated radiation and surgery in a mesothelioma mouse model. Clin Cancer Res. 2017

Statement of Translational Relevance

As the combination of immunotherapy with radiation therapy (RT) gains clinical traction, an improved understanding of mechanisms of potential synergy is important to maximize benefit. The practice of irradiating the tumor-associated draining lymph nodes (DLN), known as elective nodal irradiation (ENI), is frequently used by radiation oncologists when treating localized cancers to address potential subclinical nodal disease. It remains unknown whether irradiation of the DLN impacts combinatorial efficacy with immune checkpoint blockade (ICB). These studies show that ENI restrains the potent adaptive anti-tumor immunity that can be achieved by combining stereotactic tumor-directed RT and ICB. Mechanistically, ENI modulated chemokine signaling - leading to reduced immune infiltration as well as to an unfavorable balance between tumoricidal and immunosuppressive intratumoral immune cells (reflected in a decreased CD8 effector-to-Treg ratio). Exclusion of the DLN from the RT target volume should be examined in future clinical trials to promote synergy between ICB and RT.

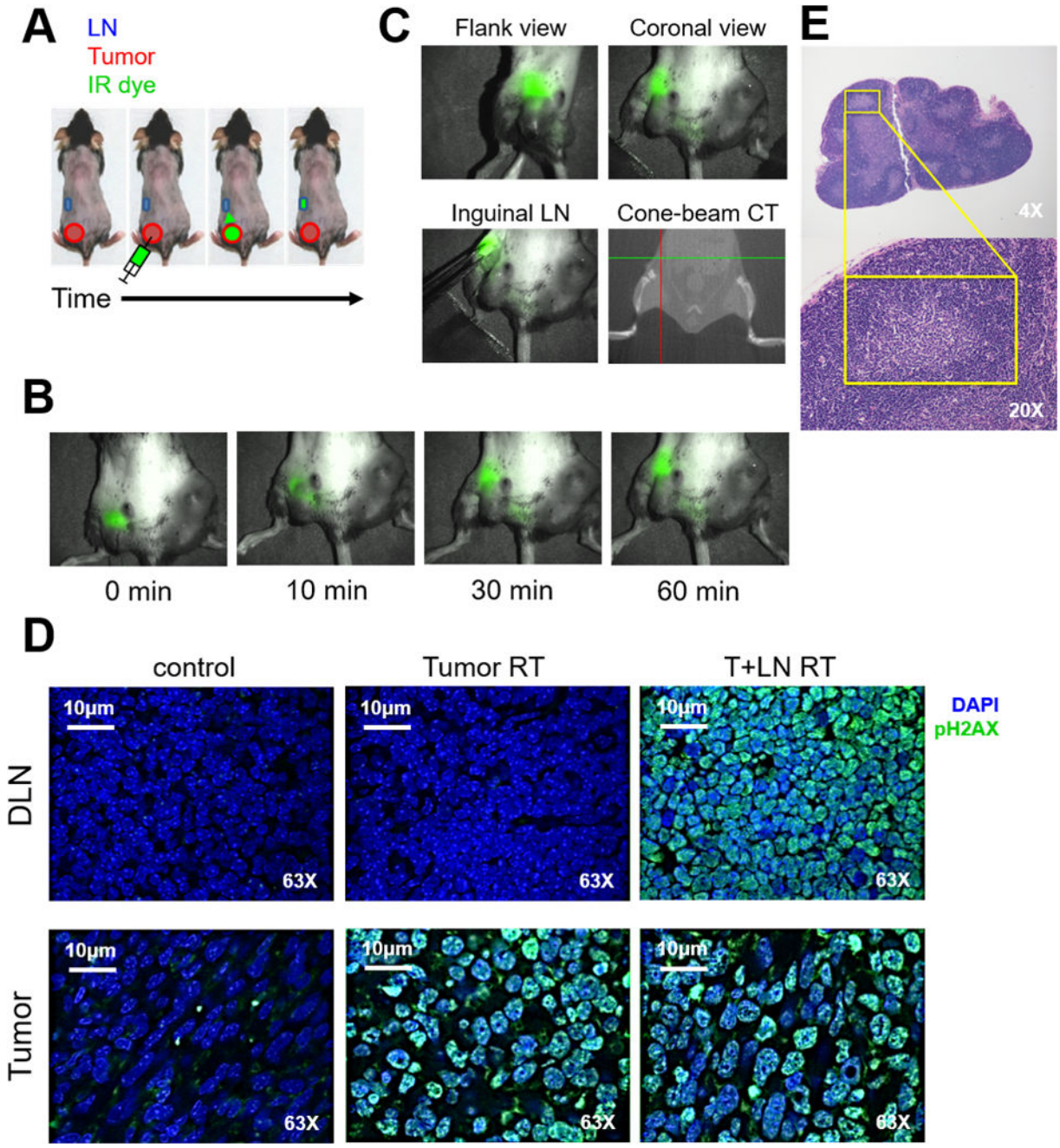

Figure 1. A preclinical model of image-guided elective nodal irradiation (ENI) accurately targets the tumor-associated DLN

(A) Lymphatic tracking of fluorescent dye (IRDye® 800CW PEG contrast agent) following intratumoral administration on day 11 in tumor-bearing C57BL/6J mice inoculated by s.c. or i.d. flank injection with 5×10^5 B16F10 or 1.5×10^6 MC38 cells (n=2-3 mice per experiment, repeated twice). **(B)** Schematic of intratumoral dye injection, transit and accumulation in ipsilateral tumor-associated inguinal lymph node (DLN). **(C)** Representative images of fluorescent dye-guided surgery isolating ipsilateral inguinal DLN and coronal view cone-beam CT image with crosshairs overlying inguinal fat pad. **(D)** Immunofluorescence

detection (63X magnification) of phospho-H2AX^{ser139} (green) and DAPI (blue) nuclear staining in non-irradiated (control) and irradiated mice (Tumor RT or T+LN RT). Tumor and DLN tissue harvested 1 hour after 12Gy x1. **(E)** Representative H&E stain (4-20X magnification) of inguinal DLN harvested from untreated B16F10 tumor-bearing mouse (n=3) on day 14 post-inoculation depicting absence of tumor cells.

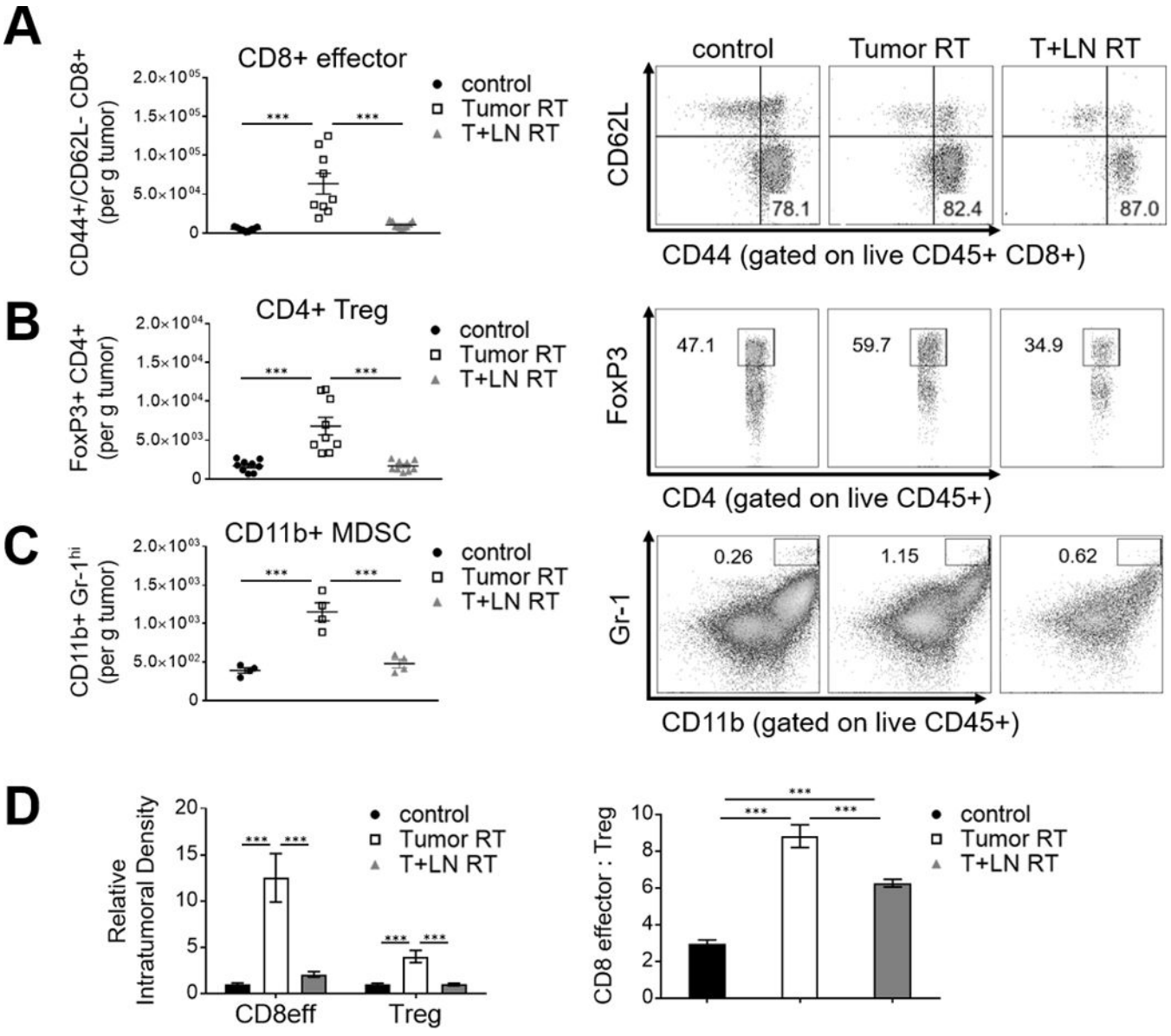

Figure 2. Elective nodal irradiation decreases tumor-infiltrating immune cell density relative to tumor-only stereotactic RT

Flank-tumor bearing mice untreated or irradiated (12Gy x1) to tumor-only (Tumor RT) or tumor and DLN (T+LN RT) on day 11 following s.c. injection of 1.5×10^6 MC38 tumor cells (n=4-9 mice per group, repeated 2-3 times). Tumors were harvested for analysis on day 16, 120 hours after treatment. **(A-C)** Representative quantitative scatterplot and flow cytometry demonstrating absolute number tumor-infiltrating immune cells and percentage (CD8+ effector, CD44+ CD62L- CD8+; Treg, CD4+ FoxP3+; myeloid derived suppressor cells, CD11b+ Gr-1^{hi}) per gram tumor in MC38 tumor model. (D) Fold change of CD8 effector and Treg subsets by treatment group, normalized to control group. Quantitative bar graph of CD8 effector-to-Treg ratio by treatment group. Error bars represent SEM, ***: $p < 0.001$, **: $p < 0.01$, *: $p < 0.05$, treatment group comparisons by one-way ANOVA and post-hoc Tukey's multiple comparison test.

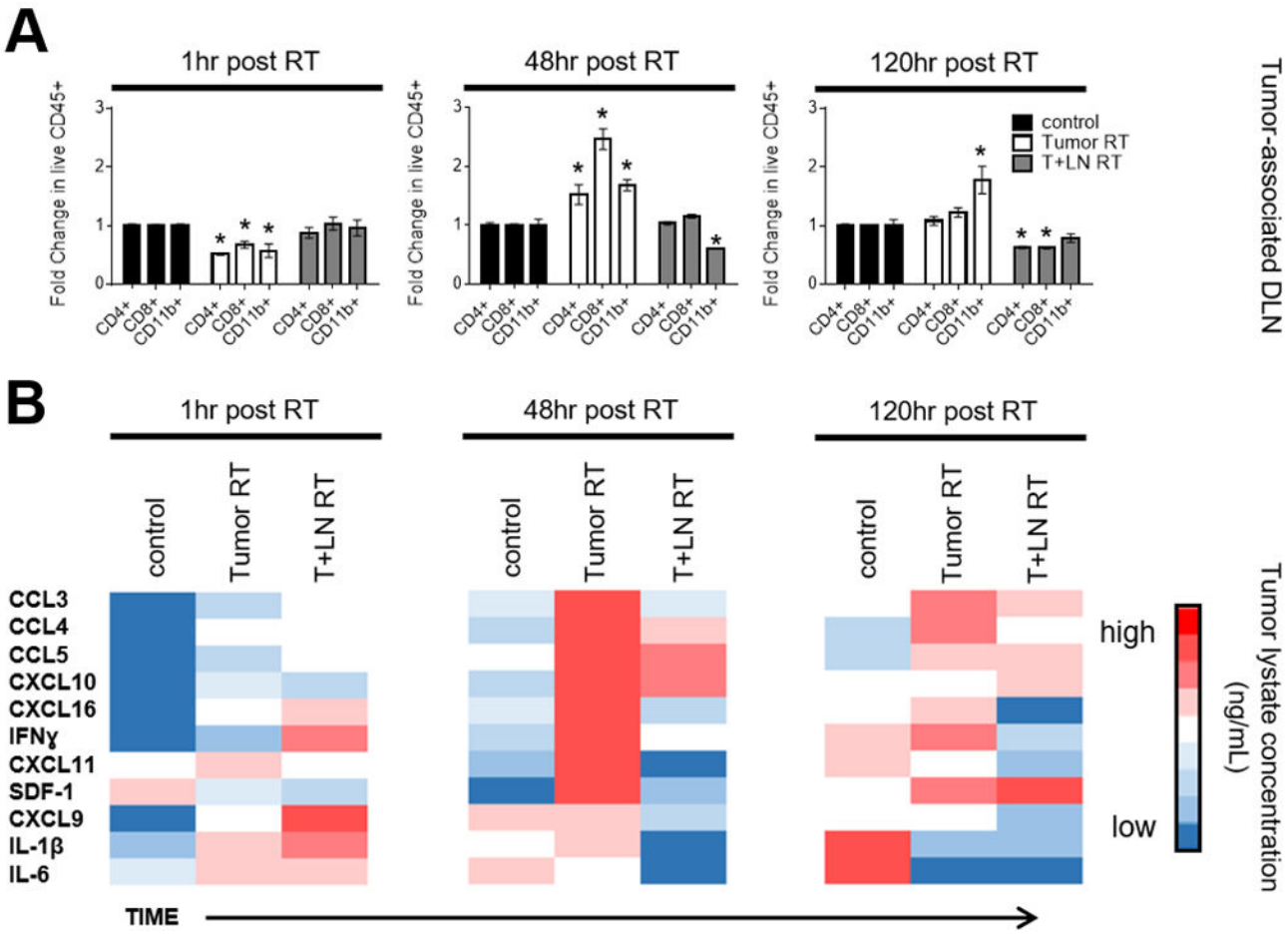

Figure 3. Tumor RT and T+LN RT have distinct radiation-induced intratumoral chemokine expression and CD8+ T-cell trafficking patterns

(A) Tumor-associated DLN of MC38 tumor-bearing mice harvested at 1hr, 48hrs and 120hrs after treatment with Tumor RT or T+LN RT on day 11. Quantitative bar graphs representing fold change of absolute number of CD4+, CD8+ and CD11b+ immune cell subsets in tumor-associated DLN over time, normalized to control (n=12 mice per group with 4 mice per time point, repeated twice). **(B)** Tumor lysate collected at same post-RT timepoints as Fig. 3A and analyzed by Luminex® multiplex immunoassay. Colorimetric heat map conditional formatting with blue to red indicating low to high chemokine/cytokine concentration [pg/mL], respectively. Error bars represent SEM, ***: $p < 0.001$, **: $p < 0.01$, *: $p < 0.05$, CD45+ immune cell and chemokine expression time course experiments analyzed by two-way ANOVA and post-hoc Tukey's multiple comparison test.

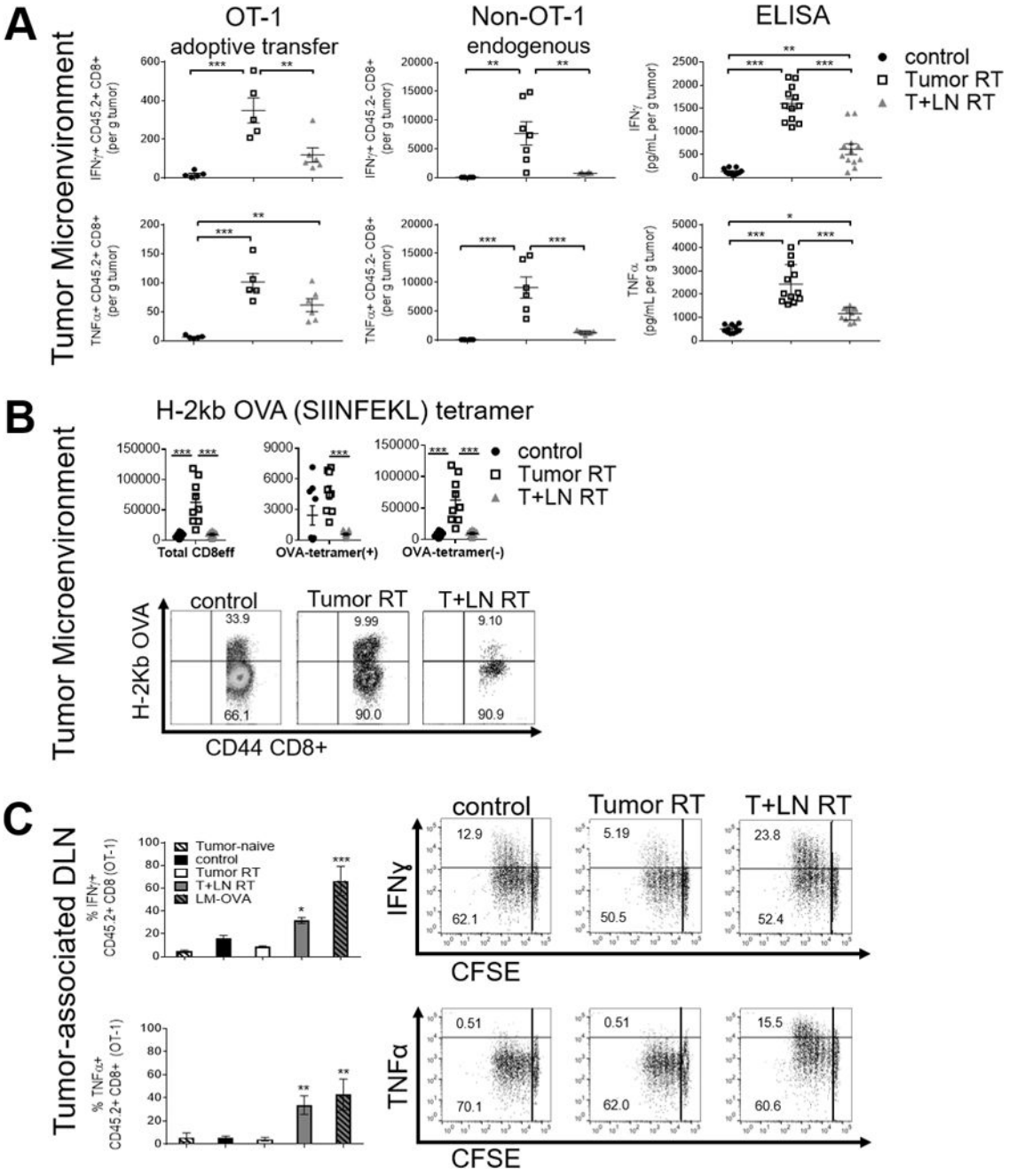

Figure 4. Radiation-mediated tumor infiltration with functional antigen-specific CD8+ T-cells is restrained by elective nodal irradiation

2×10^6 CFSE-labeled, OVA-specific CD8+ T-cells from donor $Rag^{-/-}$/OT-1 TCR transgenic CD45.2 mice were adoptively transferred (AT) into MC38-OVA tumor-bearing congenically-mismatched CD45.1 C57BL/6J mice on day 13. CD45.1 mice were treated on day 11 (48 hours before AT) with control, Tumor RT and T+LN RT with DLN and tumor harvested on day 16, 120 hours after RT (AT, n=5-9 mice per group, repeated 3 times). **(A)** Quantitative scatter plots of effector cytokine production by tumor-infiltrating OT-1, endogenous CD8+ T-cells via intracellular cytokine staining and ELISA (upper rows, L to R

respectively). **(B)** Absolute number of tumor-infiltrating CD8+ CD44+ T-cells per gram tumor by H-2kb OVA (SIINFEKL) tetramer staining and representative flow cytometry plots (ELISA and tetramer staining, n=5 per group, repeated twice). **(C)** Bar graphs and representative flow plots of effector cytokine production (IFNγ, TNFα) by AT CD45.2+ CD8+ T-cells in tumor-associated DLN. Error bars represent SEM, ***: $p < 0.001$, **: $p < 0.01$, *: $p < 0.05$, treatment group comparisons by one-way ANOVA and post-hoc Tukey's multiple comparison test.

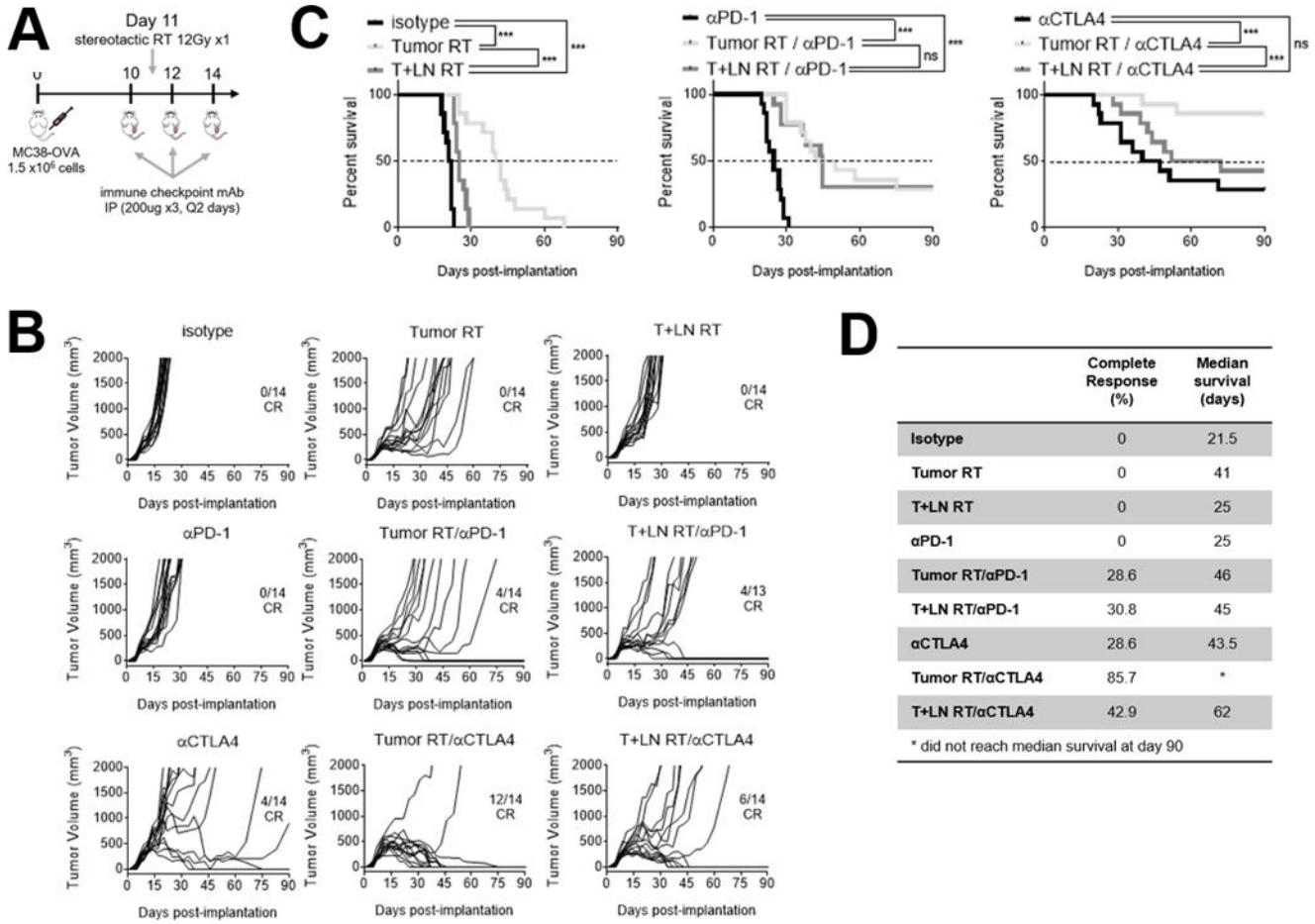

D

	Complete Response (%)	Median survival (days)
Isotype	0	21.5
Tumor RT	0	41
T+LN RT	0	25
αPD-1	0	25
Tumor RT/αPD-1	28.6	46
T+LN RT/αPD-1	30.8	45
αCTLA4	28.6	43.5
Tumor RT/αCTLA4	85.7	*
T+LN RT/αCTLA4	42.9	62

* did not reach median survival at day 90

Figure 5. Elective nodal irradiation attenuates combinatorial efficacy between radiation and immunotherapy

(A) Treatment schema; Tumor RT or T+LN RT (12Gy x1) administered on day 11 and three doses (i.p. 200μg) of therapeutic antibody (isotype, αPD-1, αCTLA4) on days 10,12,14 in MC38-OVA tumor-bearing mice (n=6-7 per group, repeated twice). **(B)** Spider plots of tumor outgrowth (mm^3) by treatment group, annotated with number of complete responses (CR) over total mice treated. **(C)** Percent survival by treatment group at day 90 after s.c. flank injection of MC38-OVA tumor cells. **(D)** Summary table of % CR and median survival by treatment corresponding to (B-C). Kaplan-Meier analysis with log-rank (Mantel-Cox) test for survival differences between treatment groups. ***: $p < 0.001$, **: $p < 0.01$, *: $p < 0.05$.

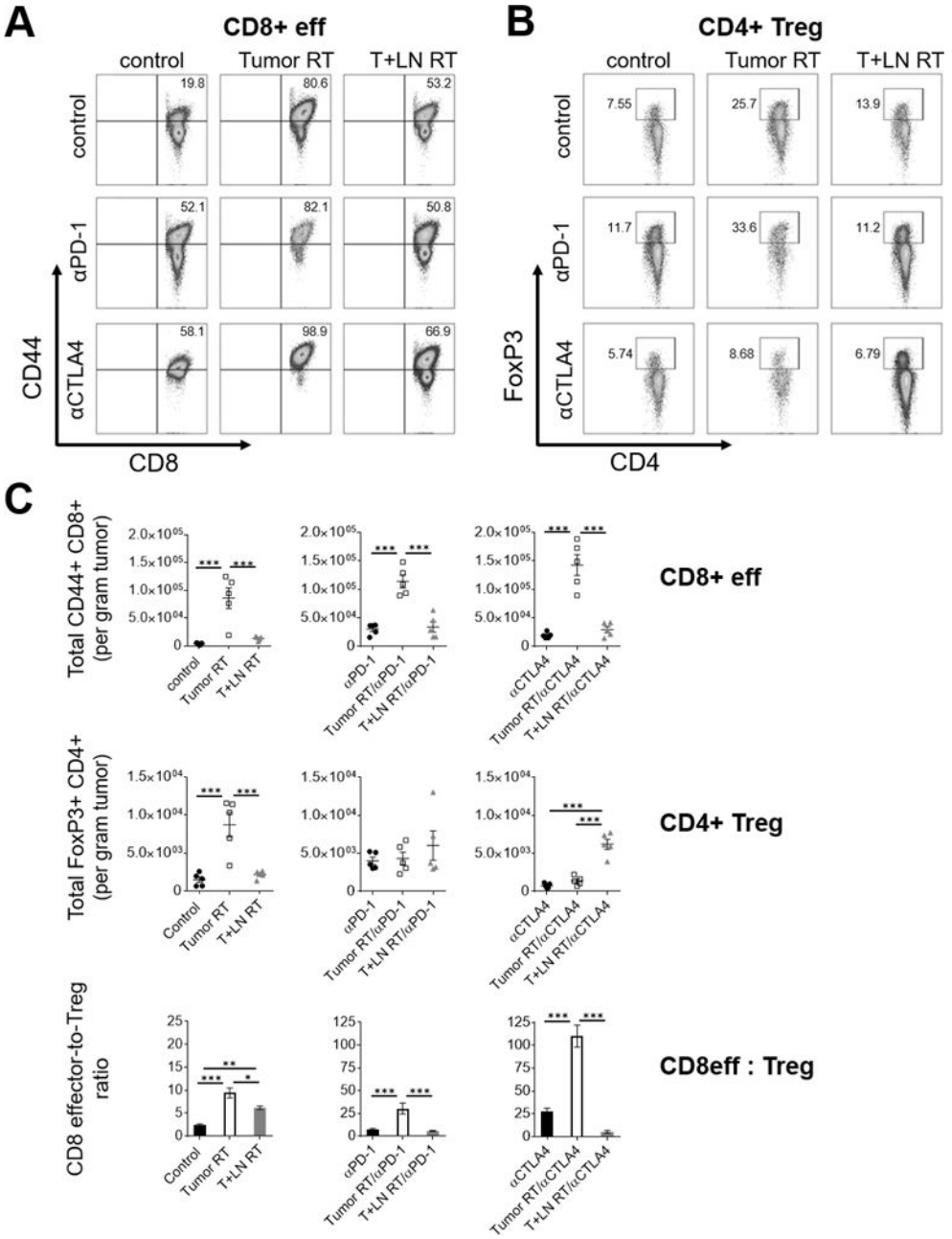

Figure 6. Favorable modulation of intratumoral CD8 effector-to-Treg ratio is associated with long-term survival

MC38-OVA tumor-bearing mice treated per schema in Fig. 5A, tumors harvested day 21 after s.c. flank injection (n=5 per group). **(A-B)** Representative flow cytometry (left, CD8 effectors; right, Tregs) and **(C)** quantitative scatterplots (upper and middle panels), demonstrating percentage and absolute number tumor-infiltrating immune cells per gram tumor by treatment group, respectively. **(C)** Quantitative bar graph (bottom panel) of CD8 effector-to-Treg ratio by treatment group. Error bars represent SEM, ***: $p < 0.001$, **: $p < 0.01$, *: $p < 0.05$, treatment group comparisons by one-way ANOVA and post-hoc Tukey's multiple comparison test.

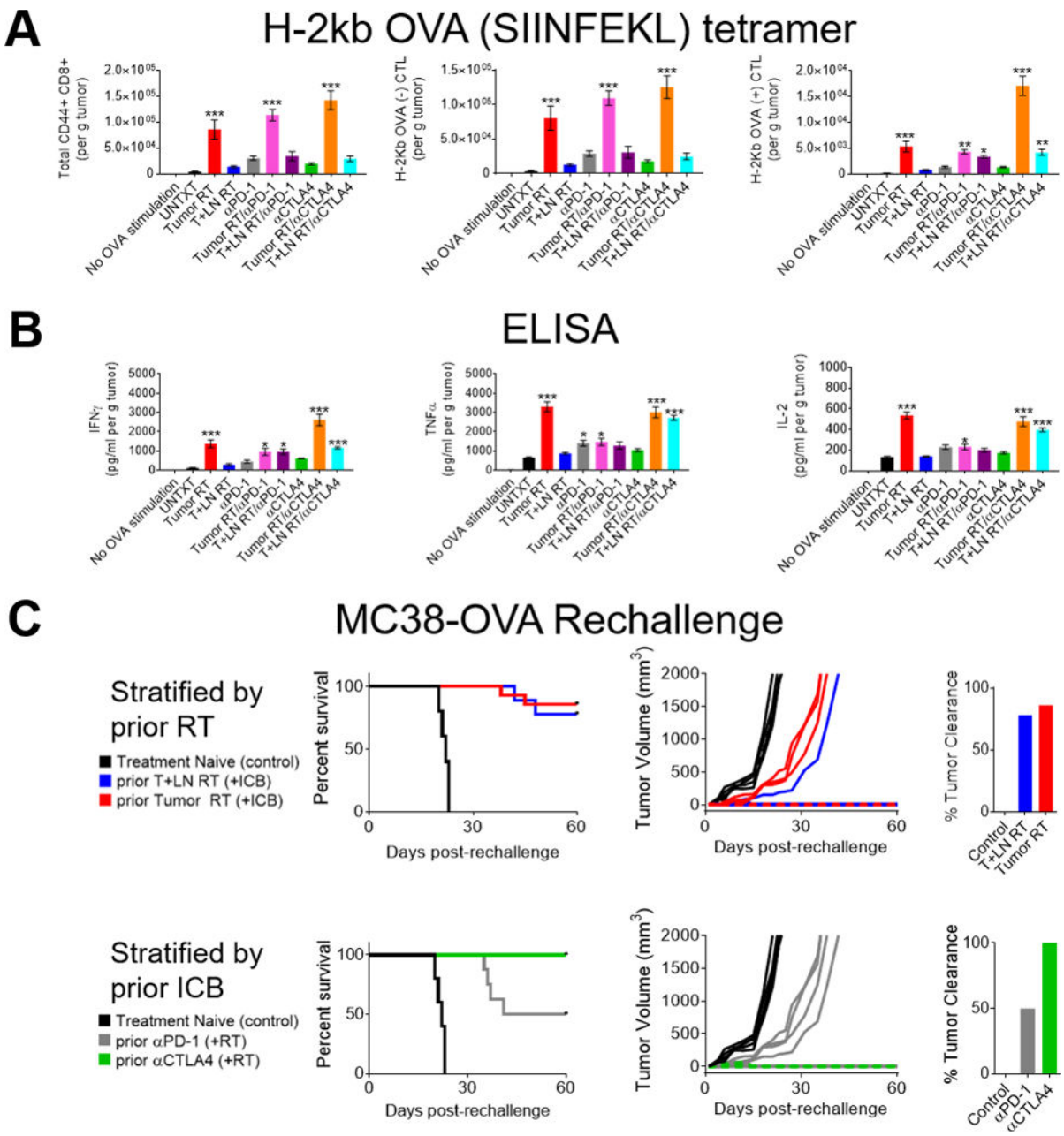

Figure 7. Improved resistance to re-challenge in animals treated with RT + αCTLA4

MC38-OVA tumor-bearing mice treated per schema in Fig. 5A. Tumors harvested day 21 after s.c. flank injection (n=5 per group). **(A)** Absolute number of antigen-specific tumor-infiltrating CD8+ CD44+ T-cells per gram tumor by H-2kb OVA (SIINFEKL) tetramer staining. **(B)** Measurement of cytokine concentration [pg/mL per gram tumor] by ELISA in TIL-derived supernatant. **(C)** Long-term survivors with complete responses previously treated with combined RT and ICB were re-challenged on the contralateral flank with 1.5×10^6 MC38-OVA tumor cells 180 days after initial tumor s.c. implant; spider plots, % survival and % tumor clearance stratified by prior RT strategy or prior ICB received (treatment-naïve, n=5; Tumor RT, n=11 vs. T+LN RT, n=9; αPD-1, n=8 vs. αCTLA4,

n=15). Error bars represent SEM, ***: $p < 0.001$, **: $p < 0.01$, *: $p < 0.05$, treatment group comparisons by one-way ANOVA and post-hoc Tukey's multiple comparison test.